Arch. Metall. Mater. **63** (2018), 4, 1827-1835

DOI: 10.24425/amm.2018.125111

J. DUTKIEWICZ*, S. RUSZ**, D. KUC***, O. HILSER**, P. BOBROWSKI*, B. KANIA*

MICROSTRUCTURE AND TEXTURE CHANGES OF MgLiAl ALLOYS COMPOSED OF α OR $\alpha + \beta$ PHASES AFTER TWIST CHANNEL ANGULAR PRESSING TCAP

Two MgLiAl alloys of composition 4.5% Li and 1.5% Al (in wt.%) composed of α phase and of 9% Li, 1.5% Al composed of α (hcp) + β (bcc) phases were subjected to twist channel angular pressing (TCAP) deformation. Such deformation of $\alpha + \beta$ alloys caused less effective grain refinement than that of single α phase alloy. However, with increasing number of passes, grain size of single α phase alloy increased and that of β phase in two phase $\alpha + \beta$ alloy also grew, which suggested the effect of dynamic recrystallization. TEM studies allowed identifying particles of Li_2MgAl phase of size of few μm. {001}<100> texture was observed in extruded alloy. Texture studies of extruded and TCAPed single phase hcp alloy indicated texture with $\{10\bar{1}0\}$ plane perpendicular to the extrusion direction and {0002} plane parallel to the extrusion direction. Duplex $\alpha + \beta$ alloys showed poor texture development.

Keywords: MgLiAl alloys; twist channel angular pressing TCAP, texture after TCAP, Li_2MgAl precipitates

1. Introduction

Mg-Li alloys show improved formability through the activation of non-basal slip systems [1], particularly the prismatic slip as confirmed by texture studies [2]. Duplex Mg-Li alloys deformed at low rolling deformation revealed strong basal texture $\{0002\}\ <1\bar{1}00>$ with the basal poles rotated around ±25° from the normal direction ND towards the rolling direction RD with the dominant $\{11\bar{2}2\}\ <1\bar{3}21>$ component in the α phase. Both, basal texture $\{0002\}\ <1\bar{1}00>$ and pyramidal component $\{11\bar{2}2\}\ <1\bar{3}21>$ strengthened with the increasing reduction of sample thickness, while the tendency for the basal poles to rotate from the ND diminished. Similar observation was reported in [3]. It showed the deviation of the $\{10\bar{1}1\}$ and $\{11\bar{2}0\}$ planes from the extrusion axis towards the horizontal plane. In the extruded β phase, the {100} planes were tilted approx. 13°-70° from the direction parallel to extrusion one towards the transverse direction and the {110} planes were often perpendicular to the extrusion direction. The addition of Li hindered the activation of $\{1012\}\ <1\bar{1}00>$ tension twinning; however the addition of aluminum decreased the resistance to that phenomenon [4]. The texture of the bcc β phase was dominated by the cubic {001}<100> component [2] and the fiber texture component (<110>//rolling direction) was very strong after 90% deformation by rolling at room temperature. However, there is evidence that the *c* fiber ({111}// rolling plane) weakened with increasing rolling strain to give a peak-like texture centered at {111}<110> crystallographic orientation [4]. The cubic texture disappeared in the β phase of the two phase alloy, replaced by the {011}<100> and {113}<332> components. Authors suggested that the strength of single hexagonal α phase alloys could be further improved by grain refinement, which was an important concept, since the other common strengthening methods, like texture control and alloying, might not be effective in that case [5]. The preferred orientations for the Mg-rich α-phase of the extruded Mg10.3Li2.4Al0.7Zn alloy were the {0001} basal planes parallel to the transverse direction and the $\{11\bar{2}0\}$ prismatic planes parallel to the normal direction [6]. Since the tensile direction during tensile tests is parallel to the basal plane, basal slip – as well as the deformation twins – will barely be present during these tests and will not contribute to the obtained ductility. It has been reported, that the addition of Li in the Mg-Li alloys to form a solid solution in the Mg matrix will decrease the length of the *c*-axis and thus lead to a reduction in the *c*/*a* ratio. This phenomenon helps to suppress the basal slip but promotes the prismatic slip [7]. Agnew et al. [8] indicated that Li additions may lower the non-basal stacking fault energy of the glissile dislocations and increase the stability of the glissile configuration. Since the pyramidal slip mode offers five independent slip systems, it provides an explanation for the improved ductility of Mg-Li alloy [6]. Two phase alloys show generally much better plasticity [9-12] and Mg8Li alloy shows excellent superplastic properties after equal channel angular pressing at 473 K and the strain rate 10^{-4} s^{-1}, with the strain rate sensitivity coefficient oscillating between 0.4-0.6 [9]. ECAP

* INSTITUTE OF METALLURGY AND MATERIALS SCIENCE, POLISH ACADEMY OF SCIENCES, 30-059 KRAKÓW UL. REYMONTA 25, POLAND
** TECHNICAL UNIVERSITY OSTRAVA, DEPARTMENT OF MECHANICAL ENGINEERING, 17 LISTOPADU 15, OSTRAVA, CZECH REPUBLIC
*** SILESIAN TECHNICAL UNIVERSITY, DEPARTMENT OF METALLURGY AND MATERIALS SCIENCE, KATOWICE UL. KRASIŃSKIEGO 8, POLAND
# Corresponding author:

processing at higher Li content with the β bcc structure have shown the substantial refinement of grains down to 200 nm and the existence of $MgLiAl_2$ precipitates due to the Al addition [9]. A very effective method of grain refinement by the high pressure torsion (HPT) was applied to the Mg8Li alloy, leading to grain refinement to the average size of 500 nm [11] and superplastic deformation ability already at 50°C or higher. A near Burgers orientation relationship was observed between the two phases, i.e. $[0001]\alpha \parallel [0\bar{1}1]\beta$ and $(1\bar{1}00)\alpha \parallel (\bar{2}11)\beta$ with an additional ~0.5° rotation of the bcc lattice around the [0001] α axis, explained by the transformation-induced increase of stress [12]. The texture evolution in a duplex Mg-Li alloy was studied in [13]. The results indicated the deformation mode transition of the hexagonal-close-packed (hcp) α phase from the basal slip to the pyramidal slip during hot-rolling to 40% of thickness reduction. The elongation to failure in tensile testing increased with decreasing extrusion temperature, while the ductility grew from low values in the as cast state, to high ones after the extrusion and ECAP. In the specimen cold-rolled with 80% reduction of thickness, strong X-ray intensities of $(200)\beta$ and $(0002)\alpha$ peaks were observed at the top surface of cold-rolled plate, indicating the $\{100\}\beta$ and $\{0002\}\alpha$ planes parallel to the rolling plane [13]. It was contrary to the results reported in [2], where the {001} component decreased at higher reductions.

During severe cold-rolling, the lattice constants of the Θ–$MgLi_2Al$ phase were found to diminish, indicating that the Mg atoms in the Θ phase were partly replaced by the Al atoms. The results showed that the grains of the matrix β phase were substantially refined, with the mean size decreasing from 60 μm to 200 nm. The distribution of the α precipitates, which were embedded in the β grains and the ternary $MgLiAl_2$ phase, was homogenized by ECAP processing. The existence of the $MgLiAl_2$ phase was confirmed using various diffraction methods [14], which disagrees with other findings, in which the $MgLi_2Al$ phase was observed [10,13].

In the present paper, a comparison of elevated temperature deformation characteristics of hexagonal α phase MgLi4.5Al1.5 alloy and two phase $\alpha + \beta$ MgLi9Al1.5 (numbers indicate wt.%) was performed. A small aluminum addition was applied to the Mg-Li alloys in order to increase their mechanical properties as reported in [15,16] and to study its effect on the grain refinement and precipitation structure in single and two phase alloys after TCAP in comparison with ECAP [17].

2. Experimental procedure

Two magnesium based alloys of composition 4.5 wt.% Li and 1.5 wt.% Al (alloy 1) intended to be α phase (hcp) and of 9 wt.% Li, 1.5 wt.% Al (alloy 2) intended to be composed of $\alpha + \beta$ (hcp + bcc) phases were cast under argon atmosphere and extruded at 350°C to obtain bars of cross section 12×12 mm foreseen for the TCAP deformation. The TCAP tool consisted of helical part in the horizontal area of the channel with angle of lead $\gamma = 30°$. The basic aim of the use of helix consisted in the simulation of back pressure and thus in the increase of extrusion force. Up to 3 TCAP passes were applied using the rotation of samples in the following passes. Alloys MgLi4.5Al1.5 and MgLi9Al1.5 of higher plasticity were deformed at 160°C and 200°C, respectively. The extrusion force was measured during the process. The hardness of samples was tested with a Zwick ZHU 250 instrument using Vickers method and the tensile tests were performed on Instron 6025 – testing machine at room and elevated temperatures using samples cut out after ECAP with an electro-spark device to thickness 2 mm and width 3.5 mm, testing length 18 mm and total length 45 mm. The structure and composition were studied using an Leica optical microscope, FEI Quanta FEG-SEM or Philips CM20 transmission electron microscope. Samples for the EBSD analysis were prepared by ion polishing in the JEOL Cross Section Polisher using Ar^+ ions at 4.0-6.0 keV energy. EBSD measurements were carried out using the FEI Quanta FEG-SEM equipped with EDAX Hikari camera. The accelerating voltage of the electron beam was 20 kV and the electron beam current was kept in the range from 16 nA to 32 nA. The orientation distribution maps were acquired from regions dimensions ranging from 15×15 μm to 50×50 μm, and the step size used was in the 50-100 nm range on a square grid pattern. The grain size using optical or TEM microscopes was estimated by the measurements in two perpendicular directions to calculate the average value. Thin samples of hot pressed or TCAPed alloys were cut by the electro spark, then dimpled and electropolished in the electrolyte consisting of 750 ml AR grade methanol, 150 ml butoxyethanol, 16.74 g magnesium perchlorate and 7.95 g lithium chloride and finally dimpled using Gatan dimpler and ion beam thinned using Leica EM RES101 ion beam thinner. The X-ray diffraction was performed using a Philips PW 1710 diffractometer with Co Kα radiation. The crystallographic texture was examined based on the pole figures obtained with a modified 7-axes Bruker D8 Discover diffractometer. Pole figures were registered using the standard Bragg-Brentano geometry, with polycapillary focusing X-ray optics and the pinhole collimator of 1.0 mm diameter working on the primary beam. The 2.6 LynxEye silicon strip detector set to 0D mode was employed for the secondary beam. The goniometer radius of the apparatus was 300.0 mm and filtered Co-K$\alpha_{1,2}$ radiation was used for all of the samples. The measurement grid for each pole figure consisted of a simple equal step grid with $\Delta\alpha = \Delta\beta = 5.0°$ and α varying from the 0° to 75°. The intensity was corrected according to the powder correction based on the reference magnesium powder sample. The {100}, {002}, {101} and {012} families of crystallographic planes were observed in the hexagonal Mg-Li phase and for the cubic Mg-Li phase – the {011}, {002} and {013} ones. The orientation distribution function (ODF) was calculated with the LaboTex 3.0 software [18] implementing the arbitrary defined cell algorithm. Shares of the specific texture components were estimated in LaboTex with the model function methods based on preliminary ODF maxima search and results were checked and visualized with the tools of the TARSIuS package [19].

3. Results and discussion

Figure 1a shows optical micrograph of alloy 1 extruded at 350°C. One can see that the grains in alloy MgLi4.5Al1.5 are of round shape indicating a partial recrystallization during the hot extrusion process. Small precipitates, reported also in previous papers, were identified as $MgLi_2Al$ or $MgLiAl_2$ [9,13], therefore their structure was examined using selected area diffraction pattern (SADP). The micrograph of extruded and TCAPed alloy is shown in Fig. 1b. The refined and elongated grains can be seen, however it is difficult to estimate the grain size due to presence of fine precipitates. The microstructure of alloy MgLi9Al1.5 was similar to that reported in two phase MgLi based alloys [2,6,7,10,12-14], with elongated lamellae of the α phase (visible as bright) within the β phase. The structure changes after TCAP (Fig. 2b) are better visible in the MgLi9Al1.5 alloy, where the partition of lamellae and refinement of the β grains can be observed, although it was also difficult to estimate their size, so the TEM studies were performed. Figure 3 shows the TEM micrograph of extruded alloy Mg4.5Mg1.5Al with a large precipitate of rectangular shape and relatively high dislocation density within the α grain, which indicates, that the recrystallization process during hot extrusion was not completed. The SADP indicates the presence of hexagonal α solid solution with 100 row excited and symmetrical orientation of the cubic precipitate at the $[01\bar{1}]$ zone axis orientation with crystal lattice confirming the presence of Li_2AlMg as was also reported in [9,12].

Table 1 shows the results of measurements of mechanical properties such as hardness HV_{10}, yield strength YS, ultimate tensile strength UTS and tensile elongation ε. It can be seen that YS and UTS are slightly higher for the samples after TCAP than for the extruded MgLi4.5Al1.5 alloy, most probably due to the grain size decrease. A small difference in the properties results presumably from the fact that both processes were carried out at elevated temperatures and the recrystallization was difficult to control due to longer time of the TCAP process. The dislocation density in the extruded and TCAPed samples was rather high. Two phase MgLi9Al1.5 alloy showed also a slight increase of UTS after ECAP, but generally the change of mechanical properties was very small for a similar reason as for the other alloy. The results are slightly different from these reported in [20], where the increase of UTS and YS after ECAP was accompanied by the significant drop of ductility, which was not observed in our case. It was probably caused by the direct ECAP deformation after casting described in [19]. Another reason influencing the mechanical properties of MgLi alloys is texture, particularly in the α phase with a lower number of slip systems, where the change of texture affects possible slip mode from the basal plane

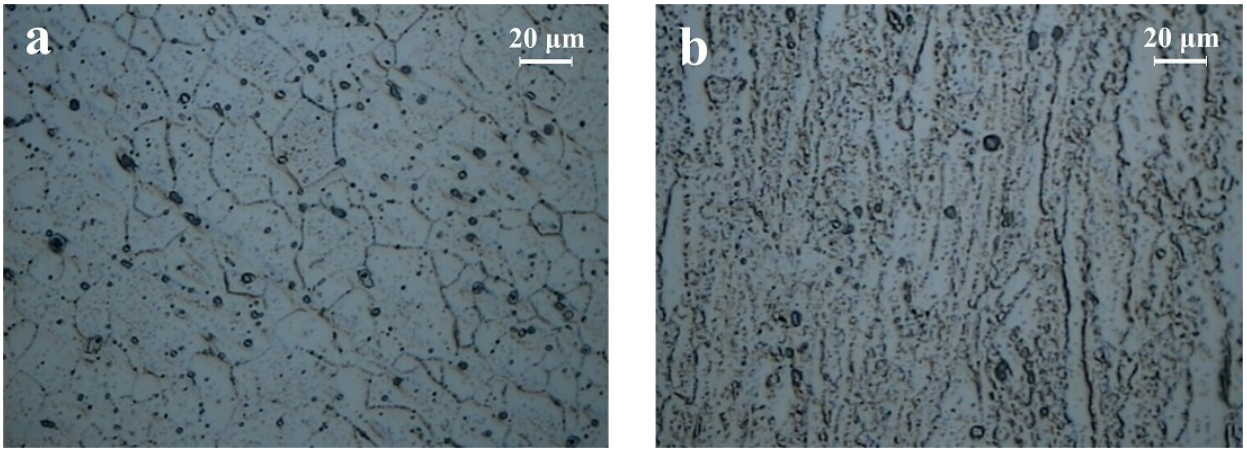

Fig. 1. (a) Optical microstructure of hot extruded alloy AlLi4.5Al1.5 and (b) The alloy after first TCAP pass

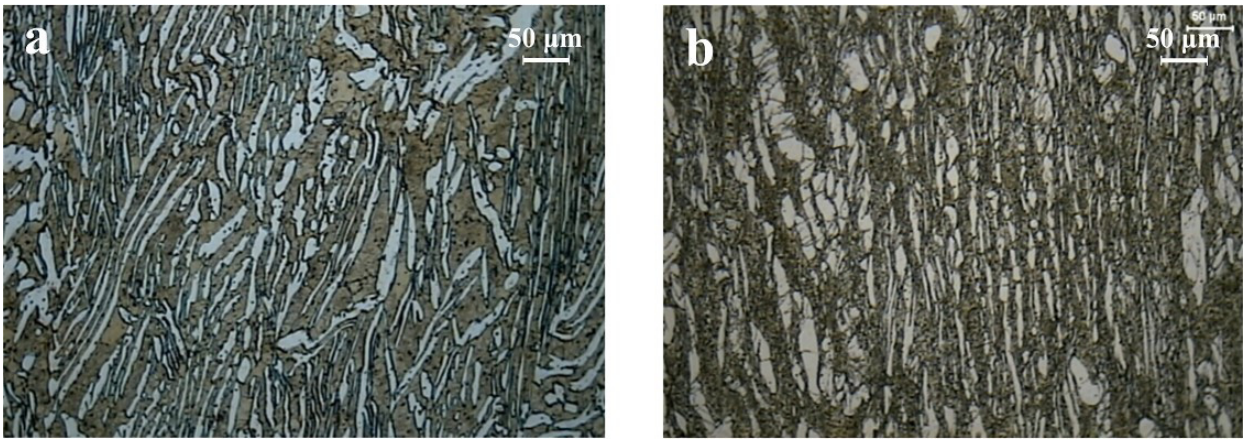

Fig. 2. (a) Optical microstructure of hot extruded alloy AlLi9Al1.5 and (b) The alloy after first TCAP pass

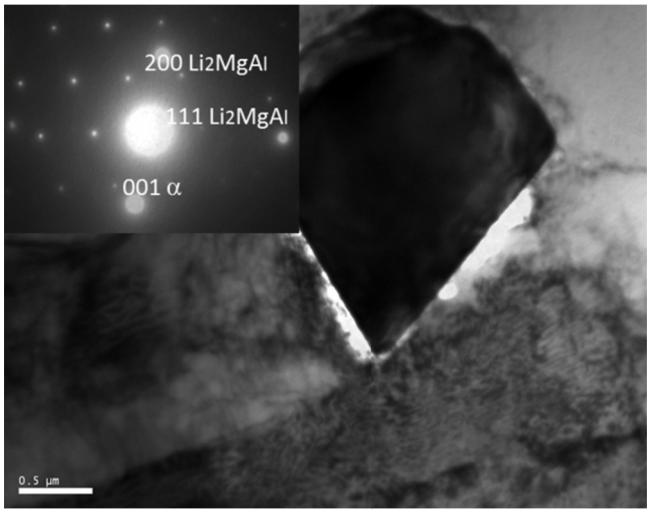

Fig. 3. TEM micrograph of extruded alloy MgLi4.5Al1.5 and selected area diffraction pattern (SADP) as an insert

to pyramidal one [2,3]. That is why, the texture alterations in the extruded and TCAPed samples of both phases are important and they were examined in the present paper. The mechanical properties were similar after extrusion and after TCAP indicating a small increase of hardness and tensile strength of the alloy MgLi4.5Al1.5, while the results for the MgLi9Al1.5 alloy were similar after both deformation modes.

TABLE 1

Results of measurements of mechanical properties

Sample	HV_{10}	YS [MPa]	UTS [MPa]	ε [%]
Alloy MgLi4,5Al1,5 extruded	70 ±3	120 ±5	195 ±7	8.5
Alloy MgLi9Al1,5 extruded	60 ±3	133 ±5	154 ±7	31.5
Alloy MgLi4,5Al1,5 after 1 TCAP pass	62 ±3	132 ±5	218 ±7	9
Alloy MgLi9Al1,5 after 1 TCAP pass	60 ±3	129 ±5	170±7	27

Figure 4 presents the TEM micrographs and SADP of alloy MgLi4.5Al1.5 after 1 and 3 TCAP passes. It can be seen, that after 1 pass the grains are elongated with rather high dislocation density. The SADP from the area shows zone axis orientation $[01\bar{1}0]\alpha$ and reflections extended toward Debye-Scherrer rings reaching the misorientation up to 5 degrees between the grains. The microstructure of the sample subjected to 3 TCAP passes reveals larger grains, showing, however, stronger contrast changes between them. The SADP from the elongated dark central grain demonstrates small misorientation up to 5° and indeed, a small contrast changes due to further refinement probably with a low angle boundaries can be distinguished within the grains in the lower part of the micrograph. In both samples rather high dislocation density occurs. The results of grain size measurement

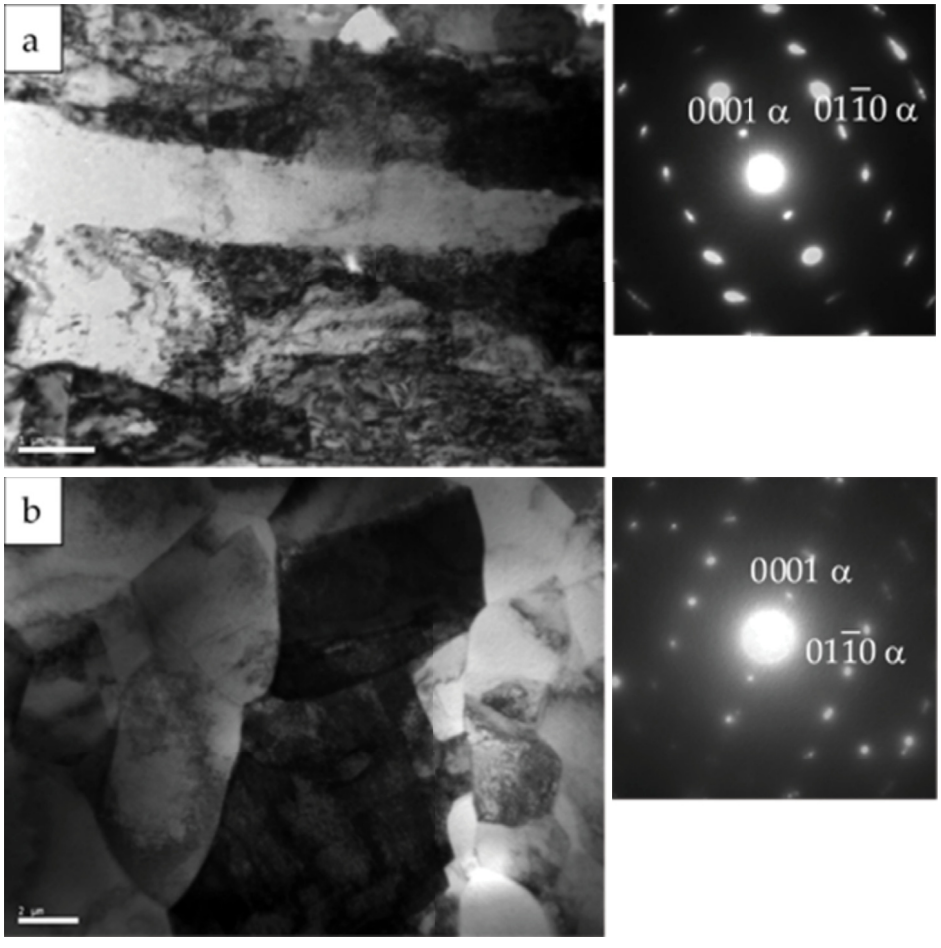

Fig. 4. (a) TEM micrographs and selected area Diffraction patterns from alloy MgLi4.5Al1.5 after 1 TCAP pass and (b) after 3 TCAP passes

for the MgLi4.5Al1.5 alloy are placed in the Table 2. They are based on the set of 50-60 grains from several TEM microstructures indicates that the grain size after one TCAP pass is 1.4 μm and increases after 3 passes up to 5.2 μm. The coalescence of initial fine grains of small misorientation into larger grains of higher misorientation is the possible mechanism; the process was accelerated by elevated temperature 220°C and contributed to the texture change.

TABLE 2

Results of grain size measurement of alloys after extrusion (optical microscopy) and after 1 and 3 TCAP passes (TEM observation)

Sample	D_α [μm]	D_β [μm]
Alloy MgLi4,5Al1,5 extruded	24	120
Alloy MgLi9Al1,5 extruded	29.6	133
Alloy MgLi4,5Al1,5 after 1 TCAP pass	1.4 (1.6 EBSD)	132
Alloy MgLi9Al1,5 after 1 TCAP pass	60	129
Alloy MgL9Al1,5 3 TCAP passes	2.1	12.3

Figure 5 shows the TEM microstructure of alloy MgLi-9Al1.5 after 1 TCAP pass. A narrow band of β grains of bright and dark contrast and size of a few μm can be seen between two α grains. The indexing of SADP pattern shows that the $[01\bar{1}0]\alpha$ and $[111]\beta$ zone axes are parallel to the electron beam. The differences between both phases are visible; rather cellular type of subgrains within the α phase and well developed grain boundaries within the β grains. In fact, the measurements presented in Table 2 show that in two phase alloy the grain refinement of the α grains is not as effective as in predominantly single phase alloy MgLi4.5Al1.5, confirming, that most probably, the deformation occurs mainly in the softer β phase, where dynamic recrystallization results in developing high angle grain boundaries. The

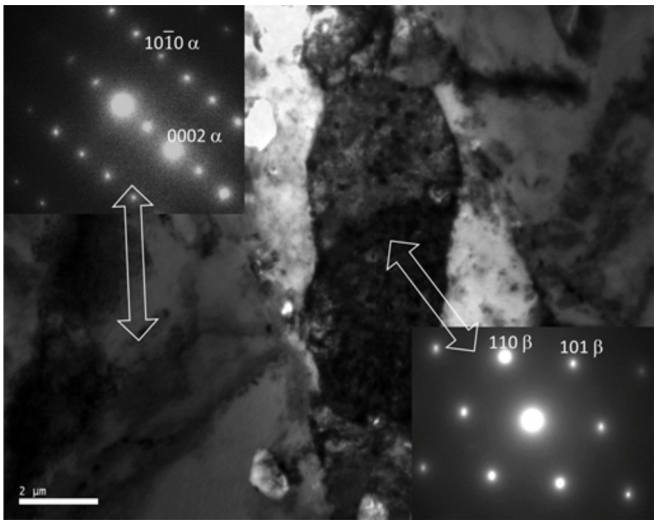

Fig. 5. TEM micrograph from the alloy MgLi9Al1.5 after 1 TCAP pass showing a band of β phase between α grains and corresponding SADP of a left α and central β phases

dislocation density is higher than in the α phase, which can be seen in this and other micrographs.

Figure 6a presents the EBSD orientation map image taken of alloy MgLi4.5Al1.5 after 1 TCAP pass. Two types of grains can be distinguished; larger ones elongated in the pressing direction (rotated in the exit helical part) and smaller equiaxial ones between them. Most of elongated grains show a small misorientation causing further grain refinement. The average grain size estimated from EBSD is 1.6 μm what is in a good agreement with the data based on the TEM grain size measurement in Table 2. The (0001) pole figure suggests that the basal plane is oriented perpendicularly to the pressing direction and, similarly to the grains, deviates from the pressing direction. Figure 6b depicts the results of EBSD studies of investigated alloy MgLi9Al1.5 after 1 TCAP pass. Some nonhomogeneity of grain size and misorientation is similar to these observed in Figure 6a. The grain size of the α phase in the duplex alloy was measured only for the α phase, while the areas of the β phase were marked mostly with gray color, because their orientations were not solved. The mean grain size of the α phase after 1 TCAP pass was calculated at 6.5 μm and that of the α phase after 3 TCAP passes at 2.1 μm. The grain size of both phases was also measured using TEM studies from the limited data of about 50-60 grains. The results after 1 TCAP pass are similar to that of EBSD; therefore the grain size measurements were performed also for another specimen and listed in Table 2. It can be seen, that grain refinement of the α phase is more intense than that of the β phase in alloy MgLi9Al1.5. With increasing number of passes the grain size of β phase rises, while that of the α phase decreases. It is most probably caused by more intense deformation of the softer β phase (confirmed also by faster electrolytic thinning of its elongated grains) and its dynamic recrystallization at elevated temperature. The hexagonal α phase reveals higher dislocation density, but it seems to carry less deformation. The α grain refinement is more pronounced in the single phase MgLi4.5Al1.5 alloy after the first TCAP pass than in the two phase alloy due to higher deformation of this phase.

Figure 7 contains the set of pole figures from extruded alloy Mg4.5Al1.5 of hexagonal α phase. The texture formed during hot pressing of square cross section rods is well developed (maximum texture intensity is 2.7) and can be defined by ideal orientations $(10\bar{1}2)$ $[\bar{3}033]$ $(03\bar{3}2)$ $[0\bar{3}39]$ and $(01\bar{1}0)$ [0001]. The results are similar to these reported in [2] and [3]. Figure 8 shows {0001} and $\{10\bar{1}0\}$ pole figures from the hex α phase of extruded alloy and {001} and {110} pole figures from the bcc β phase of the as extruded duplex MgLi9Al1.5 alloy. They acquired different ideal orientations than those of the α phase in Figure 7 and similar to reported in [2] and [3]. (β phase {100} planes perpendicular to the extrusion direction, $\{0001\}\alpha$ planes parallel to it.).

Figure 9 presents pole figures $\{10\bar{1}0\}$ and (001) of the sample extruded and after 1 TCAP pass. Different rotation of poles after 1st and 3rd pass results from the BC rotation and additional one of crystals in the exit helical part. Comparing $\{10\bar{1}0\}$ pole figures of plane after extrusion and TCAP pass, it is visible, that

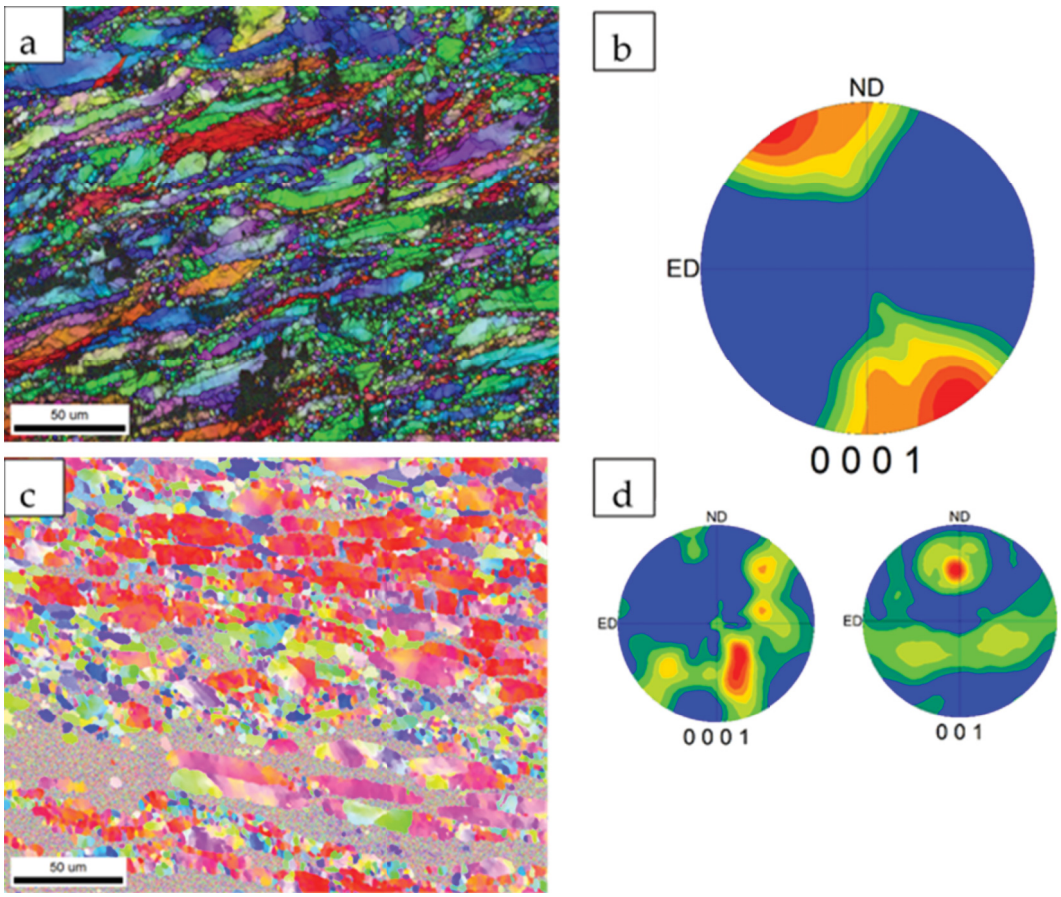

Fig. 6. (a) EBSD image taken from the alloy MgLi4.5Al1.5 after 1 TCAP pass; (b) 0001 pole figure calculated from EBSD studies (c) EBSD image from the alloy MgLi9Al1.5 after 1 TCAP pass; (d) 0001 α and 001 β pole figures calculated from EBSD studies

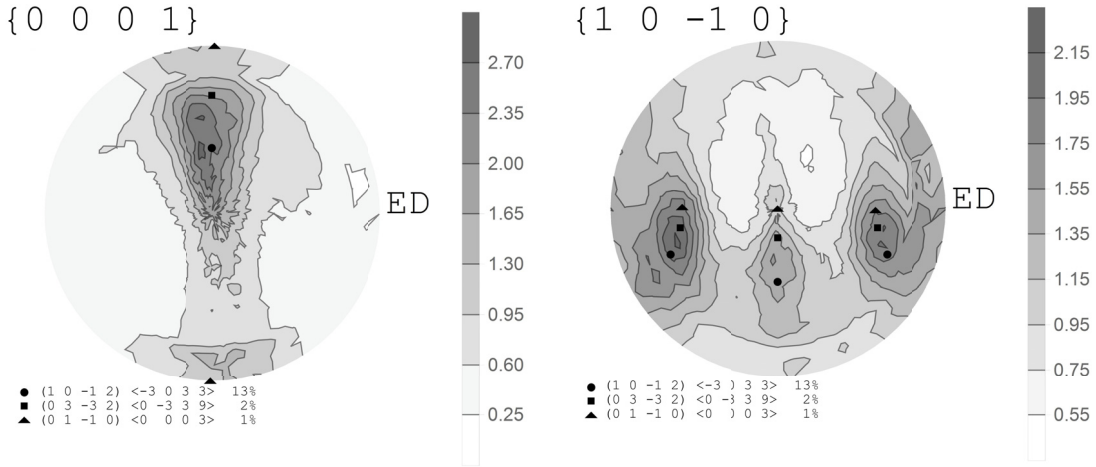

Fig 7. {0001} and {10$\bar{1}$0} pole figures from extruded alloy Al4,5Al1,5 of hexagonal α phase. Circle, squares and triangles show poles (10$\bar{1}$2) [$\bar{3}$033] (03$\bar{3}$2) [0$\bar{3}$39] and (01$\bar{1}$0) [0001] ideal orientations respectively

the pole rotates around the extrusion direction and also around the perpendicular direction. The {10$\bar{1}$0} planes became perpendicular to the extrusion direction. The similar type of {0002} textures was observed in the ZK60 alloy after ECAP with {0001} planes parallel to the extrusion direction, in which the angle of rotation around <0001> direction was found to be dependent on the ECAP temperature [21]. Higher degree of deformation by 3 TCAP passes caused the stabilization of {001} plane as parallel to the extrusion direction and that of {100} perpendicular to the extrusion one. The pole figures after 3 TCAP were similar to that reported for the ZK60 alloy after ECAP [21].

Pole figures of hcp and bcc phases in the duplex alloy after 3 TCAP passes are shown in Figure 11. They do not show similarity to these of the hcp α phase after 1 or 3 TCAP passes presented in Figs. 9 and 10, where the {10$\bar{1}$0} plane was perpendicular to the extrusion direction and {0001} one was parallel to it. In

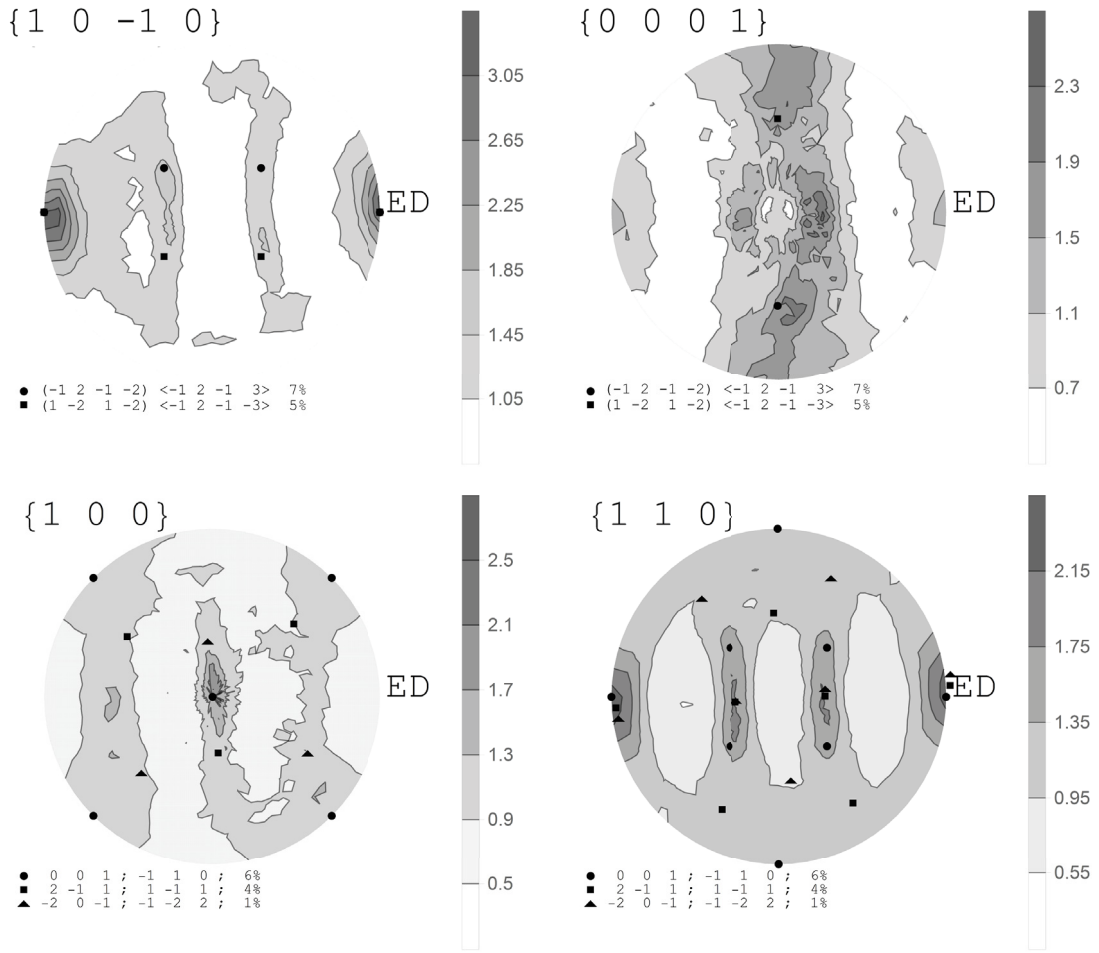

Fig. 8. Upper row shows {0001} and {10$\bar{1}$0} pole figures from hexagonal α phase of extruded alloy MgLi9Al1.5. Circle and squares show poles ($\bar{1}2\bar{1}$ $\bar{2}$) [$\bar{1}2\bar{1}3$] and ($1\bar{2}12$) [$\bar{1}2\bar{1}3$] with extrusion direction (ED) parallel to <$\bar{1}2\bar{1}3$> direction. Below (100) and (110) pole figure taken from bcc phase. Ideal orientations (001)[$\bar{1}$10], ($2\bar{1}1$)[$1\bar{1}1$] and ($\bar{2}0\bar{1}$)[$\bar{1}$ $\bar{2}$2] are marked as circles, squares and triangles respectively

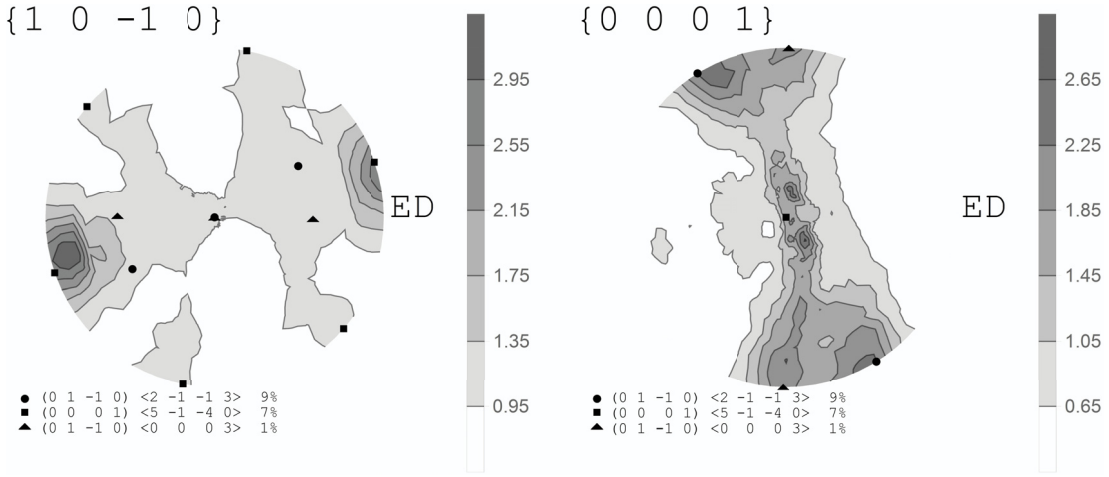

Fig. 9. {10$\bar{1}$0} and {0001}pole figures from extruded alloy Al4.5Al1.5 after 1 TCAP pass. Circles, squares and triangles show main orientation poles ($\bar{1}2\bar{1}$ $\bar{1}$)[$\bar{1}2\bar{1}6$] and ($32\bar{5}$ $\bar{1}$)[$\bar{5}7\bar{2}9$]

fact, the pole figures, particularly of hcp α phase indicate close to random orientation with diffused maxima and the maximum intensity peak near 1.5. Concerning the bcc β phase, the texture is slightly more developed, however it is difficult to compare with the textures after ECAP since they are not available for the MgLi alloys. The (110) pole figure is similar to the reported annealing texture reported in [3] of a duplex MgLi alloy, which may confirm the TEM observation of a possibility of dynamical recrystallization of the β phase due to its easier deformation than that of the α phase.

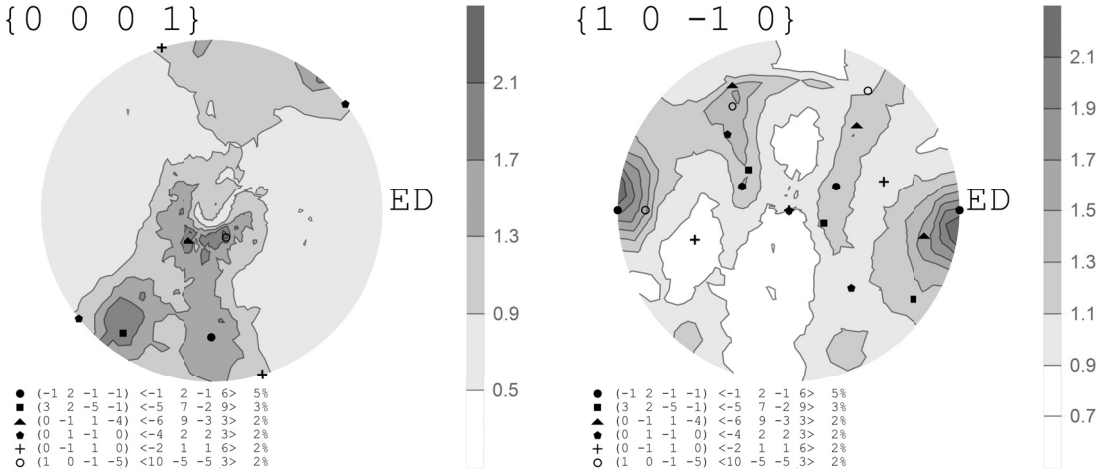

Fig. 10. Upper row shows {100} and {001} pole figures from alloy MgLi4,5Al1,5 after 3 TCAP passes. Circle and squares show poles $(\bar{1}2\bar{1}1)$ $[01\bar{1}2]$, $(32\bar{5}1)[\bar{1}13\bar{2}3]$, $(0\bar{1}1\bar{4})[\bar{1}4\bar{3}1]$, $(0\bar{1}10)$ $[\bar{2}021]$ and $(12\bar{3}\,\bar{5})[50\bar{5}1]$

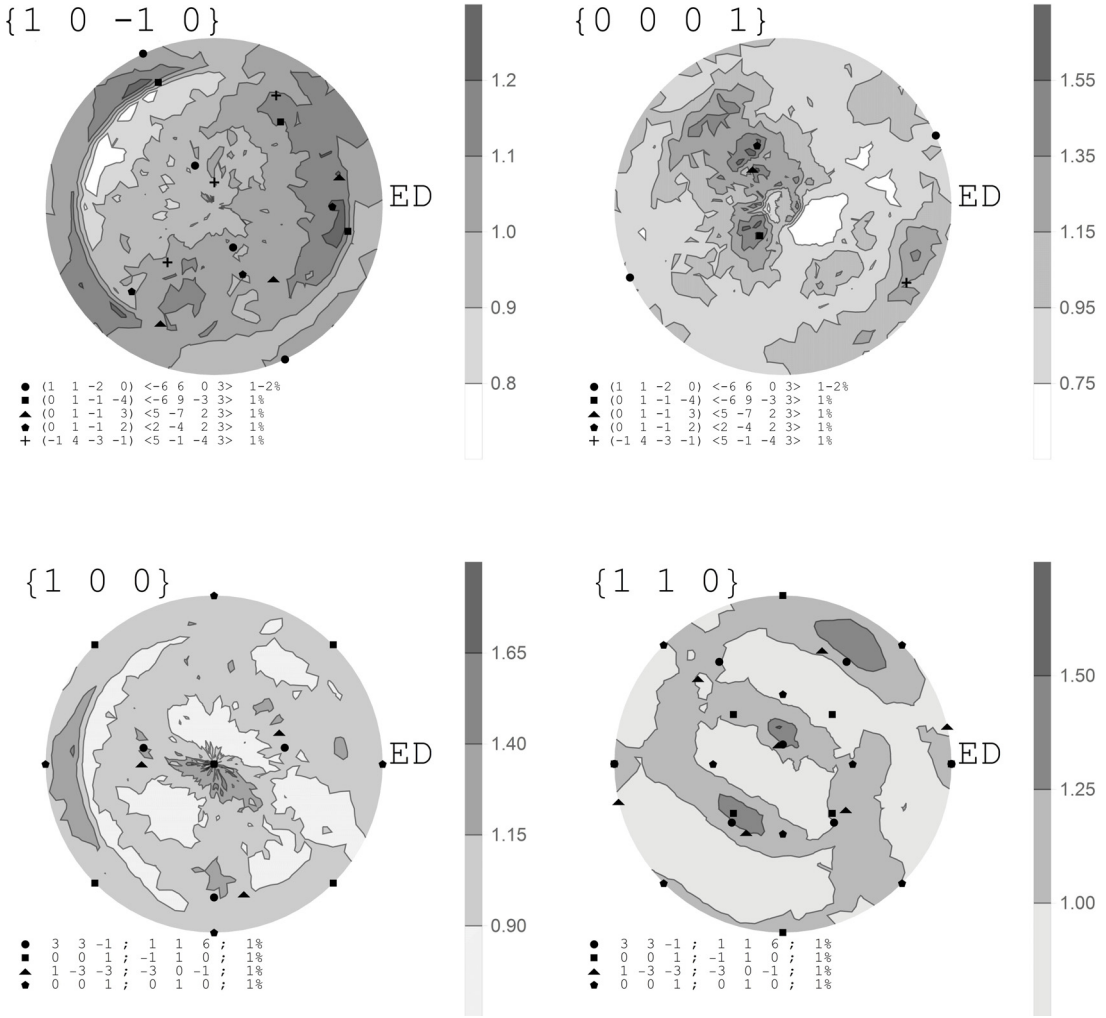

Fig. 11. Upper row shows {100} and {001} pole figures of hexagonal α phase from alloy MgLi9Al1,5 after 3 TCAP passes. Circles, squares, triangles, pentagon show poles $(11\bar{2}0)$ $[\bar{2}201]$, $(01\bar{1}\,\bar{4})[\bar{1}4\bar{3}1]$, $(01\bar{1}3)[1\bar{3}21]$, $(01\bar{1}2)$ $[0\bar{2}21]$ and $(\bar{1}4\bar{3}\,\bar{1})[31\bar{4}1]$. Below (100) and (110) pole figures from the cubic β phase with marked ideal orientations $(33\bar{1})[116]$, $(001)[\bar{1}10]$, $(1\bar{3}\,\bar{3}\,)[\bar{3}0\bar{1}]$ and $(001)[010]$

4. Conclusions

1. TCAP deformation at temperatures 160°C of $\alpha + \beta$ alloys caused less effective grain refinement than that of single α phase alloy at 200°C. However, with increasing number of passes, grain size of single α phase alloy increased and that of β phase in two phase $\alpha + \beta$ alloy also grew, which suggested the effect of dynamic recrystallization after increasing number of passes. Grain size of α phase in duplex alloy slightly decreased what might be caused by lower deformation since the β phase transferred majority of deformation as was supported by TEM microstructures. Hardness and yield stress of both alloys did not change much after TCAP passes as compared with the extruded alloy, which also confirmed the presence of dynamic recrystallization.
2. TEM studies allowed identifying particles of Li_2MgAl phase of size of few μm, which were refined below 1 μm after TCAP passes. Higher density of precipitates was observed within β phase probably due to its higher lithium content. Crystallographic relationship (0001) α || (110) β was observed very often and small particles of the α phase were incorporated into the β phase after 3rd TCAP pass.
3. $\{0001\}\langle 10\bar{1}0\rangle$ texture was observed in the present study in extruded alloy in agreement with previous texture studies of extruded or rolled hcp MgLi based alloys. Texture studies of extruded and TCAPed single phase hcp alloy indicated texture with $\{10\bar{1}0\}$ plane perpendicular to the extrusion direction and {0002} plane parallel to the extrusion direction in agreement with literature reports on ECAPed magnesium alloys. Duplex $\alpha + \beta$ alloys showed poor texture development with increasing number of TCAP passes, although the β phase revealed presence of recrystallization texture supporting TEM observation of dynamic recrystallization appearing with increasing number of TCAP passes at relatively low deformation temperature of 160°C.

Acknowledgements

The financial support of the OPUS research project No. 2014/15/B/ST8/03184 and PRELUDIUM research project No. 2015/17/N/ST8/02320 both funded by the National Science Centre NCN is gratefully acknowledged.

REFERENCES

[1] S.R. Agnew, J.W. Senn, J.A. Horton, JOM **58**, 62-69 (2006).
[2] Y. Zou, L. Zhang, H. Wang, X. Tong, M. Zhang, Z. Zhang, J. Alloys Compd. **669**, 72-78 (2016).
[3] Y. Tang, Q. Le, W. Jia, L. Fu, X. Liu, J. Cui, Mater. Sci. Eng. A **704**, 344-359 (2017).
[4] G.J. Shen, B.J. Duggan, Metall. Mater. Trans. A **38A**, 2594-2601 (2017).
[5] M. Lentz, M. Klaus, I.J. Beyerlein, M. Zecevic, W. Reimers, M. Knezevic, Acta Mater. **86**, 254-268
[6] C.W. Yang, T.-S. Lui, L.-H. Chen, H.-E. Hung, Scripta Mater. **61**, 1141-1144 (2009).
[7] F.E. Hausner, P.R. Landon, J.E. Dorn, Trans. ASM **50**, 856 (1958).
[8] S.R. Agnew, J.A. Horton, M.H. Yoo, Metall. Mater.Trans. A **33A**, 851 (2002).
[9] M. Furui, Ch. Xu, T. Aida, M. Inoue, H. Anada, T.G. Langdon, Mater. Sci. Eng. A **410-411**, 439-442 (2005).
[10] T. Liu, S.D. Wu, S.X. Li, P.J. Li, Mater. Sci. Eng. A **460-461**, 499-503 (2007).
[11] H. Matsunoshita, K. Edalati, M. Furui, Z. Horita, Mater. Sci. Eng. A **640**, 443-448 (2015).
[12] M.V. Kral, B.C. Muddle, J.F. Nie, Mater. Sci. Eng. A **460-461**, 227-232 (2007).
[13] M. Furui, H. Kitamura, H. Anada, T.G. Langdon, Acta Materialia **55**, 1083-1091 (2007).
[14] H. Dong, F. Pan, B. Jiang, R. Li, X. Huang, Mater Design **65**, 42-49 (2015).
[15] S.K. Wu, Y.H. Li, K.T. Chien, C. Chien, C.S. Yang, J. Alloy Compds. **563**, 234-241b (2013).
[16] G.H. Park, J.T. Kim, H.J. Park, Y.S. Kim, H.J. Jeong, N. Lee, Y. Seo, J.Y. Suh, H.T. Son, W.-M. Wang, J. M. Park, K.B. Kim, J. Alloy Compds. **680**, 116-120 (2016).
[17] R. Kocich, J. Fiala, I. Szurman, A. Macháčková, M. Mihola, J. Materials Sci. **46**, 7865-7876 (2011).
[18] K. Pawlik, Phys. Stat. Sol. (b) **134**. 477-483 (1986).
[19] B. Kania, P. Indyka, L. Tarkowski, E. Beltowska-Lehman, J. Applied Cryst. **48** (1), 71-78 (2015).
[20] T.-C. Chang, J.-Y. Wang b, C.-L. Chu, S. Lee, Mater. Lett. **60**, 3272-3276 (2006).
[21] E. Mostaed, M. Hashempour, A. Fabrizi, D. Dellasega, M. Bestett, F. Bonollo, M. Vedani, J. Mech. Beh. Bio. Mater. **37**, 307-322 (2014).